

Electron Paramagnetic Resonance Investigation of Ga-vacancies in β -Ga₂O₃: Experiment and Theory

Dmitry Skachkov and Walter R. L. Lambrecht
*Department of Physics, Case Western Reserve University,
10900 Euclid Avenue, Cleveland, OH-44106-7079, U.S.A.*

Hans Jürgen von Bardeleben
*Sorbonne Universités, UPMC Université Paris 06, UMR7588,
Institut des Nanosciences de Paris, 4 place Jussieu, 75005 Paris, France*

Uwe Gerstmann
Lehrstuhl für Theoretische Physik, Universität Paderborn, 33098 Paderborn, Germany

Quoc Duy Ho and Peter Deák
*Bremen Center for Computational Materials Science,
University of Bremen, P.O. Box 330440, D-28334 Bremen, Germany*

Density functional theory calculations of the magnetic resonance fingerprint of a wide variety of native defect models and their complexes are carried out using the Gauge Including Projector Augmented Wave method in order to determine the origin of the two electron paramagnetic resonance (EPR) $S = 1/2$ spectra observed in high-energy particle irradiated β -Ga₂O₃ single crystals. The first of these (EPR1) can be observed at room temperature and below and is characterized by the Spin Hamiltonian parameters $g_b = 2.0313$, $g_c = 2.0079$, $g_{a*} = 2.0025$ and a quasi isotropic hyperfine interaction with two equivalent Ga neighbors of 14 G (on ⁶⁹Ga and correspondingly 17.8 G on ⁷¹Ga in their natural abundances). The second center (EPR2) is observed after photoexcitation (with threshold 2.8 eV) at low temperature and is characterized by $g_b = 2.0064$, $g_c = 2.0464$, $g_{a*} = 2.0024$ and a quasi isotropic hyperfine interaction with two equivalent Ga neighbors of 10 G. A spin $S = 1$ spectrum with a similar g-tensor and a 50% reduced hyperfine splitting accompanies each of these, which is indicative of a defect of two weakly coupled $S = 1/2$ centers. Ga-vacancies on both octahedral and tetrahedral sites and their complexes with Ga-interstitials, the split interstitial oxygen and a self-trapped hole are considered in the modeling. The $V_{\text{Ga1}} - \text{Ga}_{\text{ib}} - V_{\text{Ga1}}$ model has the best matching g -tensor principal component directions with EPR1. Given the Fermi level not too far below the conduction band minimum it provides lower energy than the simple V_{Ga1} model in the EPR active $S = 1/2$ and $S = 1$ states than V_{Ga2} or other complexes. The latter are less likely to occur in the EPR active state because of their deeper $2 - /3-$ transition levels. A metastable state of V_{Ga2} with spin located on O off the mirror plane is a promising model to explain the EPR2 spectrum as well as its accompanying $S = 1$ state even though its hyperfine splitting would then correspond to two slightly nonequivalent Ga atoms. An oxygen trapped hole (OTH) on a split-interstitial O-dumbbell is also considered as a relevant candidate for EPR2 but less likely to be in the EPR active state and exhibits hyperfine with 3 Ga. The self-trapped hole without any additional defect, previously suggested, is excluded on the same basis.

I. INTRODUCTION

Monoclinic β -Ga₂O₃ has recently attracted attention as an ultra-wide-band-gap semiconductor.¹ Its band gap of about 4.7 eV²⁻⁶ combined with unintentionally doped semiconducting rather than insulating properties make it attractive for high-power electronics applications. Mostly, the wide band gap leads to a high breakdown field (estimated to be possibly as high as 8 MV/cm based on the relation between band gap and break down voltage in other materials, and already demonstrated⁷ to be as high as 3.8 MV/cm), plays an important role in various figures of merit (FOM) for high-power transistor design, such as Baliga's FOM.⁸ Its good transparency in the ultraviolet region also make it suitable as a transparent conductor.⁹ The origin of unintentional doping and the limitations on the degree of n-type doping that can be achieved de-

pends on a thorough understanding of the defect physics. While a substantial amount of work has already appeared on the defect physics,¹⁰⁻¹⁵ the experimental signatures of many of the defects are still unclear.

Recently, an Electron Paramagnetic Resonance (EPR) center was reported by Kananen *et al.*¹⁶ in neutron irradiated samples and ascribed to the octahedral Ga-vacancy site. In β -Ga₂O₃ there are two nonequivalent Ga sites one with a tetrahedral coordination (Ga₁) and one with an octahedral coordination (Ga₂).¹⁷ Likewise, there are three distinct O sites, O₁ and O₂ are each connected to three Ga while O₃ is connected to four Ga (see Fig. 1).

Here we present an EPR study of β -Ga₂O₃ with defects introduced by high energy particle irradiation combined with first-principles calculations of the hyperfine (HF) and g -tensors. A similar spectrum to that of Ref. 16 is observed after irradiation in the dark. After photoexcita-

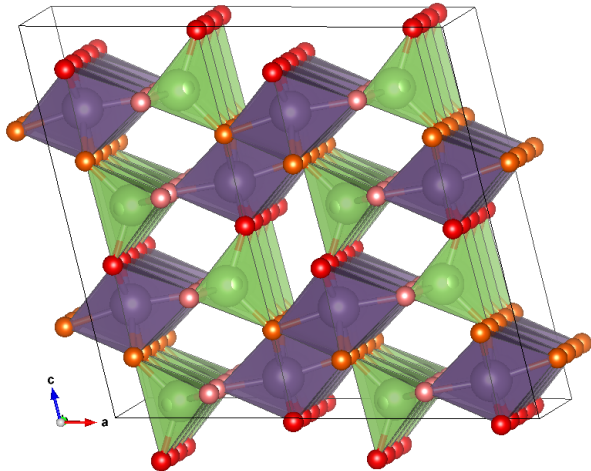


FIG. 1. Crystal structure of β -Ga₂O₃ shown in the 160 atom supercell indicating the polyhedra surrounding tetrahedral Ga₁ (in green) and octahedral Ga₂ (purple). The O₁, O₂, O₃ are colored coded as red, pink and orange.

tion a different center appears with different orientation of the main g -tensor axes and slightly smaller HF-values. That EPR center has properties similar to those previously ascribed to the self-trapped hole (STH),¹⁸ which similarly has spin density localized on an oxygen p -orbital but would not involve a Ga-vacancy. It was previously observed after X-ray irradiation at low temperature on already neutron irradiated samples. Two distinct $S = 1$ spectra are also reported here. The characteristic g -tensors and hyperfine splitting of these centers and their thermal stability are studied.

Second, we present first-principles calculations for a wide variety of native defect models in an attempt to more definitively identify the chemical nature of the observed defect centers. Given that the spectra clearly correspond to spin-density located on O sites, and that under irradiation both vacancies and interstitials of both Ga and O atoms are likely to occur, we focus on Ga-vacancies and O-interstitials. Besides the individual Ga-vacancies we also consider models in which a Ga-vacancy pair is combined with a Ga-interstitial. Such models occur naturally by the migration of a Ga to an interstitial site in the center of the hexagonal rings in which already a V_{Ga} is present. These models were found to have low energy (depending on the charge state) and low migration energy barriers compared to the individual vacancies.^{10,19} Importantly, we found that the $V_{\text{Ga}_2}^{2-}$ has a metastable state which has spin located on a pair of O off the mirror plane compared to its ground state in which the spin is located on an O on the mirror plane. In fact, which of the two has lower energy depends on the size of the supercell but we assume the larger supercell to have the more accurate energetic ordering of these two states. We will show that this model is a good candidate for the

photo-excited state.

Based on previous suggestions in the literature, self-trapped holes on two types of O are considered but ruled out on the basis that their hyperfine would be with three Ga instead of two. Oxygen interstitials occur in a split-interstitial configuration in which an O₂ dumbbell is located on an O site. We also consider this model as a candidate for O-localized spin density. Depending on how much the spin is spread over the two O in the dumbbell or remains on one, the hyperfine could be on 2 or 3 Ga. Relatedly we also consider the possibility of removing the third Ga, *i.e.* we consider an O_{*i*} – V_{Ga} complex, so as to enforce hyperfine interaction with only two Ga.

For all these models, the structure is first fully relaxed. Next their hyperfine splitting and g -tensors are calculated. The latter is calculated using the Gauge Including Projector Augmented Wave (GIPAW) method,^{20,21} which is based on a self-consistent density functional perturbation theory providing the linear (magnetic) response of the defect system onto external magnetic fields. At present we are restricted to semilocal density functionals for this part of the calculation, which presents a limitation on their accuracy as we find that the localization of the wave functions is insufficient in these functionals based on the hyperfine results. However, the g -tensor is a more global property of the defect, which is less sensitive to the localization than hyperfine interaction and good results for g -tensors to within an uncertainty of a few 0.001 were obtained in previous work for a variety of defects, at the semilocal DFT level.^{22–24} We therefore focus more on the qualitative aspects of the g -tensor, namely the orientations of the principal axes of the g -tensor which can be understood to some extent on the basis of the orientation of the spin-density. The calculated results for the various models are then compared with experiment, the merits and problems of each of the models are discussed including consideration of their expected charge states and hence EPR active or inactive state of the defect.

II. EXPERIMENTAL DETAILS

Single crystals of n-type non-intentionally doped β -Ga₂O₃ have been purchased from a commercial supplier (Tamura, Japan). The sample thickness was 500 μm and the size $4 \times 4 \text{ mm}^2$ with the **b**-axis normal to the sample plane. The samples have been irradiated at room temperature with high energy electrons or protons to introduce intrinsic defects. Typical fluences were 10^{16} cm^{-2} . The EPR spectra were taken with an X-band spectrometer (resonant frequency 9.3 GHz) and a variable temperature (4K-300K) cryostat, which allowed in-situ optical excitation. Angular variations of the EPR spectra were measured in three crystal planes. In addition to the irradiation induced defect, the samples presented EPR spectra from a shallow donor and a weak Fe³⁺ spectrum, which will not be discussed here.

III. COMPUTATIONAL METHOD

The g -tensor is calculated using the GIPAW method^{20,21,25,26} which provides a Density Functional Theory (DFT) based method to calculate the linear magnetic response of periodic system onto external magnetic fields as implemented in the code QE-GIPAW,²⁷ which is integrated within the Quantum Espresso package.²⁸ The DFT is used with various exchange-correlation functionals: the generalized gradient approximation (GGA) as parametrized by Perdew-Burke-Ernzerhof²⁹ (PBE), the same with added Hubbard- U on O- p and a hybrid functional^{30–32} with adjusted fraction $\alpha = 0.26$ of screened exchange with screening parameter $\mu = 0.00$.¹⁵ The Quantum Espresso package's³³ PWSCF code is used to obtain the self-consistent charge and spin densities and defect wave functions. While the initial relaxations of the V_{Ga} models were done with the HSE(0.26,0.00) with parameters chosen as in Ref.15 and using the Vienna *Ab initio* Simulation Package (VASP)^{34–36} the GIPAW g -tensor was only possible with the PBE functional. The hyperfine calculations in the GIPAW code were done with PBE+ U with various values of U but typically $U = 4$ eV and some of the additional models were relaxed also with the PBE+ U model.

The defects were simulated using periodic boundary conditions in a 160 and 240 atom supercells, which are respectively a $1 \times 4 \times 2$ and $1 \times 4 \times 3$ superlattices of the 20 atom conventional cell of the base-centered $C2/m$ -spacegroup β -Ga₂O₃ structure.¹⁷ The plane wave expansion was used with a cut-off of 100 Ry and the Brillouin integration used the Γ -point only for the self-consistent calculations and hyperfine structure. Convergence was tested by also using a $2 \times 2 \times 2$ shifted mesh. For the g -tensor calculations, which are more sensitive to \mathbf{k} -point convergence, the latter was used and convergence was tested by also using a $3 \times 3 \times 3$ mesh in a few test cases. Troulier-Martins type pseudopotentials obtained within the PBE exchange correlation functional were used. The hyperfine parameters were also calculated using the QE-GIPAW code.²⁷ The relativistic hyperfine tensor consists of the isotropic Fermi contact term which requires the spin density within a distance of the Thomas radius ($r_T = Ze^2/mc^2$) from the nuclear sites as well as the dipolar terms.³⁷ Within a pseudopotential or projector augmented wave approach, a reconstruction of the all-electron wave functions from the pseudo wave functions is required.³⁸ The core relaxation³⁹ was found to be small for Ga but is substantial for O hyperfine parameters. The hyperfine Fermi contact terms is sensitive to the localization of the wave function. This depends strongly on the exchange-correlation functional used. To obtain the best agreement with experiment in terms of the hyperfine values, a value as large as $U = 8$ eV is needed within the GGA+ U model. The hole wave function is thereby localized more strongly on O and the hyperfine with the neighboring Ga atoms is reduced.

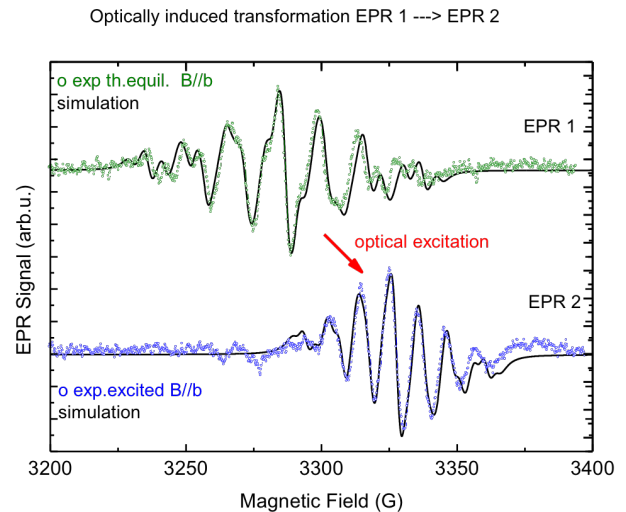


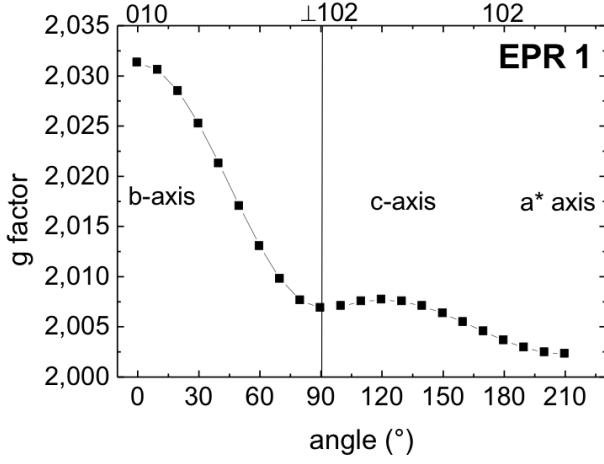
FIG. 2. Experimental and simulated EPR spectra in β -Ga₂O₃ for $\mathbf{B} \parallel \mathbf{b}$ before photoexcitation (green) at $T = 300$ K and after photoexcitation (blue) at $T = 52$ K.

IV. EXPERIMENTAL RESULTS

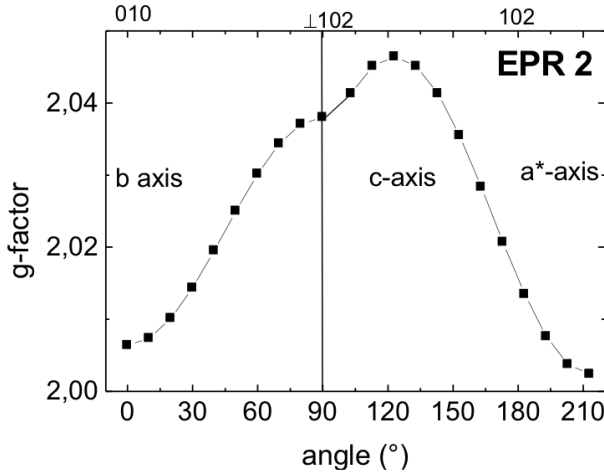
In Fig. 2 we show the EPR spectra of the irradiation induced defect center for the applied magnetic field oriented $\mathbf{B} \parallel \mathbf{b}$ both before and after photoexcitation. We call these spectra respectively EPR1 and EPR2. EPR1 occurs in the dark already at room temperature. It displays a well-resolved multiplet structure which can be simulated by a spin $S = 1/2$ center, interacting with two equivalent Ga neighbors. Due to the presence of two Ga isotopes (⁶⁹Ga, ⁷¹Ga) both with nuclear spin $I = 3/2$ but different isotopic abundances (60.1%/39.9%) and different nuclear moments in these non isotopically modified samples, the hyperfine interaction gives rise to a characteristic lineshape structure (the simulation is shown in Fig. 2). It clearly agrees with the spectrum reported previously by Kananen *et al.*¹⁶

When the sample is photoexcited at low temperature ($T < 100$ K) the spectrum EPR1 is erased and replaced by a different spectrum, EPR2, which is metastable up to a temperature of $T = 100$ K, at which the EPR1 spectrum is regenerated. The angular variation of EPR1 and EPR2 in two planes is shown in Fig.3. Fig.4 shows the crystallographic directions relative to the sample. The main parameters extracted from the fit are summarized in Table I. The spectral dependence of the photoexcitation process is shown in Fig. 5 and shows the transition occurs for photon energies larger than 2.8 eV

The particular g -values and the superhyperfine interaction with two equivalent Ga neighbors indicate for both centers a defect localized on a single oxygen site with two nearest Ga neighbors and are thus most likely associated with Ga vacancy defects, which will be further substantiated by means of the calculations. The single spin $S = 1/2$ nature of the spectrum indicates the V_{Ga} is in the $q = -2$ charge state. The various one electron lev-



(a)



(b)

FIG. 3. Angular variation of the g -factor for the variation of the magnetic field in two crystal planes for (a) EPR1 (before) and (b) EPR2 (after) photoexcitation.

els in the gap closely above the valence band maximum (VBM) would be completely filled in the $q = -3$ charge state, so that the $q = -2$ charge state has a single hole. The O hyperfine is not seen because the ^{16}O isotope has no nuclear spin and is $> 99\%$ abundant. The ^{17}O isotope with a spin of $I = 5/2$ has a natural abundance of only 3.8×10^{-4} . The hyperfine splitting is thus really a superhyperfine splitting.

Each of the $S = 1/2$ spectra reported above is accompanied by a corresponding distinct $S = 1$ spectrum. See Fig. 6. While the first $S = 1$ spectrum related to EPR1 was also previously reported by Kananen¹⁶ we here emphasize that there are two distinct $S = 1$ spectra. Each has a g -tensor equal to the corresponding $S = 1/2$ and a hyperfine splitting with about half the value of the contact hyperfine interaction for the $S = 1/2$. This suggests two weakly interacting $S = 1/2$ spins. It suggests the same defect can exist in two charge states with either one or two holes. The zero-field splitting depends on the

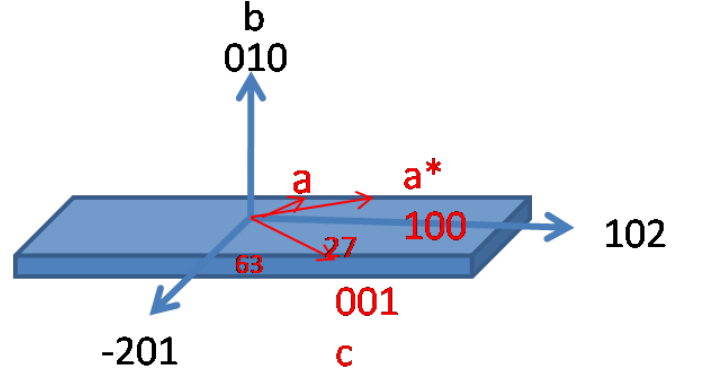


FIG. 4. Sample indicating crystal orientations.

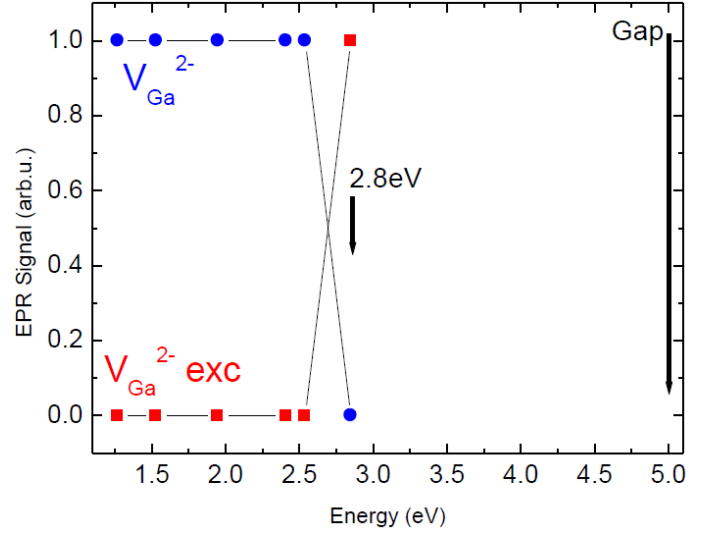


FIG. 5. Photoexcitation spectral dependence; EPR signal intensity as function of photon energy.

magnetic field direction but the full angular dependence has not yet been possible to map out because of the overlap with the main EPR1 spectrum for some directions. The order of magnitude of the zero-field splitting is consistent with the work of Kananen *et al.*¹⁶ and within a dipole approximation, indicates a well defined distance between the two spins of order 4–5 Å.

V. COMPUTATIONAL MODELS

Several models were investigated computationally by first relaxing their structures, then calculating their g -tensor and hyperfine splitting. These are: (M1) $V_{\text{Ga}1}$ with spin localized on O_1 neighbor, (M2) $V_{\text{Ga}2}$ with the spin localized on O_2 on the mirror-plane, (M3) a $V_{\text{Ga}2}$ with spin localized on two O_1 on either side of the mirror plane. The DFT+U approach in which we add a Hubbard-U on O- p orbitals proves convenient for this

TABLE I. EPR parameters g -tensor and hyperfine A tensor for ^{69}Ga . \mathbf{b} , \mathbf{c} are the axes of the conventional unit cell, \mathbf{a}^* is the axis in the b -plane at 90° from the \mathbf{c} -axis. These are close to the principal axes of the g -tensor. The HF parameters for the ^{71}Ga are obtained by multiplying by the ratio of their gyromagnetic factors which is 1.27059.

Dark	
g_b	2.0313
g_c	2.0079
g_{a^*}	2.0025
A_b (G)	13.8
A_c (G)	14.6
A_{a^*} (G)	12.8
Photoexcited	
g_c	2.0464
g_{a^*}	2.0024
g_b	2.0064
A_b (G)	9.8
A_c (G)	9.4
A_{a^*} (G)	9.0

TABLE II. Total energy differences of Ga vacancies and their stoichiometrically equivalent complexes in different charge states relative to the $q = 0$ state of V_{Ga1} .

q	0	-1	-2	-3
V_{Ga1}	0	4.62	9.96	16.25
V_{Ga2}	0.68	4.77	9.84	15.67
$V_{\text{Ga1}} - \text{Ga}_{ic} - V_{\text{Ga1}}$	0.99	4.91	9.70	15.10
$V_{\text{Ga1}} - \text{Ga}_{ib} - V_{\text{Ga1}}$	0.33	3.89	9.38	15.54

purpose. It helps us to control on which O the spin tends to localize. The total energies of these slightly different variants of the same defect were found to be close to each other. Specifically, for the V_{Ga2} whether model M2 or M3 has the lower total energy depends on the supercell size with the largest cell favoring the more symmetric model M2.

Next, we consider complexes such as the $V_{\text{Ga1}} - \text{Ga}_{ib} - V_{\text{Ga1}}$ complex, which we label M4. Figures of the models including the results of the spin density appear in the next section. The latter was found to have lower energy than a simple V_{Ga1} by Varley *et al.*¹⁰ and could occur by means of a Ga diffusion process.¹⁹ There are actually two nonequivalent such complexes, as defined in Fig. 4 of Kyrtos *et al.*¹⁹. The M4 model corresponds to the one indicated as the b location of the interstitial Ga. The two O_1 on which the spins localizes and which are related by a center of inversion at b in this case have each two Ga_2 neighbors. In the other case, indicated by c in Fig. 4 of Ref. 19 the spins localize on O_3 type atoms which have each three Ga neighbors. Our total energy calculations using the HSE hybrid functional¹⁵ (shown in Table II) indicate that this (c)-model has the lowest energy among the complexes for the $q = -3$ charge. However, for the EPR relevant charge states $q = -2$ and $q = -1$ the (b)-model has the lowest energy. Furthermore the (c)-model

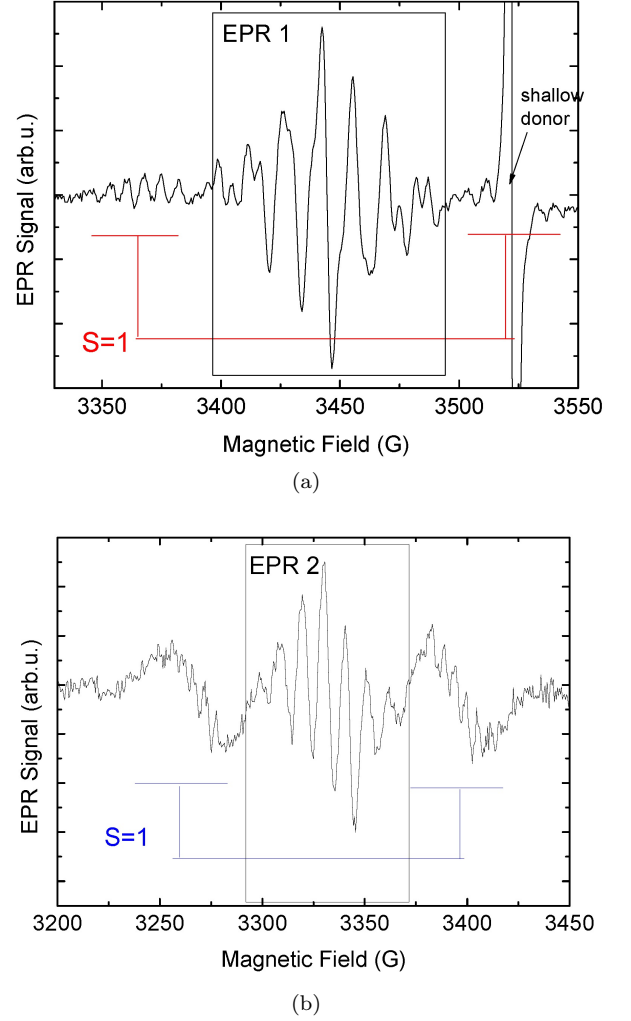


FIG. 6. $S = 1$ spectra accompanying the $S = 1/2$ (a) before photoexcitation for $\mathbf{B} \perp \mathbf{b}$ and (b) after photoexcitation for $\mathbf{B} \parallel \mathbf{b}$.

is not a plausible model for the observed EPR spectra because of the predicted hyperfine with two sets of 3 Ga instead of 2 Ga. We will later discuss their likelihood of being in the $q = -2$ or $q = -1$ charge states which are relevant as EPR active states. We have nonetheless considered both so, we will refer to the latter as the M5 model. Another complex consists of $V_{\text{Ga1}} - \text{Ga}_{ia} - V_{\text{Ga2}}$ is called the M6 model. We found for the M4 complex that the spin stays localized on one O_1 similar to the simple V_{Ga1} model and as a result exhibits slightly different relaxation near each V_{Ga1} . Nevertheless we also study a model in which the structure is constrained to stay symmetric and with spin delocalized over the two O_1 (M4'). This simulates the possibility that the spin dynamically switches back and forth from one site to the other on the time scale of the EPR experiment.

We consider two self-trapped hole (STH) models with the hole trapped either on O_1 ^{11,15} (M7) or on two O_2 (M8).¹⁵ The former has two Ga_2 and one Ga_1 neighbor.

If the latter is far enough removed due to the relaxations around the hole, then it is a plausible model for the EPR centers at hand. We will show however that the hyperfine on the third Ga is actually higher than the first two. The latter model has already spin distributed over two O₂ atoms and is thus likely to cause hyperfine on more Ga. We find below that this is indeed the case and this rules out that model. Self-trapping on O₃ was not found to occur in previous studies.¹⁵ We also note that the STH models are unlikely because the self-trapped energy level is within about 0.5 eV from the VBM and thus too deep to be EPR active with an assumed Fermi level in the upper half or near the middle of the gap.

As a variant of these models, we next consider the O_i which is, in fact, a split interstitial. It consists of an O₂ dumbbell. Among such models, the O₂ located on the O₁ site is the most promising. In fact, in the neutral charge state, it was found to be oriented close to the **c** direction. A metastable state occurs when a hole is added to this defect in this configuration. We call it an oxygen trapped hole (OTH). We label this as M9. Eventually, its ground state has the dumbbell rotated closer to the **b** direction. However, the **c**-oriented dumbbell with single hole spin located on it is an attractive model for EPR2 because the spin might become more localized near one of the two O and thereby reducing the hyperfine interaction with the third Ga, which is a Ga₁. As a final related system, we consider the O_i - V_{Ga1} complex in which that Ga₁ is removed. This is labeled the M10 model.

VI. COMPUTATIONAL RESULTS

The *g*-tensors principal values and axes as well as the HF splittings are summarized in Table III for Ga-vacancy related models (M1-M6) and in Table IV for the self-trapped and interstitial O related models (M7-M10). For the *g*-tensor calculations, we used the wave functions or self-consistent spin density calculated in PBE because the current version of the method does not yet properly handle PBE+U or hybrid functionals. On the other hand for the hyperfine calculations, we used a PBE+U model because the hyperfine is very sensitive to the degree of localization of the wave function. The higher the *U* added on the O-2p, the more the spin density becomes localized and hence it reduces the weight on the neighboring Ga atoms and reduces the HF splitting. All values in the table correspond to *U* = 4 eV.

The spin density, *g*-tensor and atoms with large HFI are shown in two views for V_{Ga1} (M1) in Fig. 7 and for V_{Ga2} (M2) in Fig. 8. The results for the V_{Ga1} - Ga_{ib} - V_{Ga1} complex (M4') is shown in Fig. 9 while those of M5, M6 are shown in Supplementary Information.⁴⁰

TABLE III. Calculated EPR parameters for various Ga-vacancy related models. For each model, we give a brief description, and the size of the cell used in the first column, the O on which the spin is localized in column 2. Under *g*-tensor we give the Δg_i (difference from the free electron *g*-value) principal values ordered from high to low and their corresponding directions, specified by their polar angle θ_i from the $\hat{\mathbf{z}} = \mathbf{b}$ axis and azimuthal angle ϕ_i from the $\hat{\mathbf{x}} = \mathbf{a}_*$ axis, both in $^\circ$, followed by which crystal axes are closest to these directions. For the hyperfine interaction HFI, we specify the number of Ga atoms with strong HFI and the isotropic component of the *A* tensor (in 10^{-4} T=Gauss). The first two lines give the experimental Δg and *A* and directions of the *g*-tensor.

Model	O	<i>g</i> -tensor			HFI	
description cell	type	Δg_1 θ_1 ϕ_1	Δg_2 θ_2 ϕ_2	Δg_3 θ_3 ϕ_3	#Ga	<i>A</i> (G)
EPR1		0.0289 <i>b</i>	0.0056 <i>c</i>	0.0002 <i>a</i> *	2	13.7
EPR2		0.0441 <i>c</i>	0.0041 <i>b</i>	0.0001 <i>a</i> *	2	9.4
M1 V _{Ga1} 160	O ₁	0.0219 0 <i>b</i>	0.0175 90 <i>a</i> *	0.0045 90 <i>c</i>	2	-22
M1 V _{Ga1} 240	O ₁	0.0228 7 19 <i>b</i>	0.0187 83 26 <i>a</i> *	0.0051 89 -64 <i>c</i>		
M2 V _{Ga2} 160	O ₂	0.0235 0 <i>b</i>	0.0161 90 <i>a</i> *	0.0062 90 <i>c</i>	2	-22
M2 V _{Ga2} 240	O ₂	0.0202 4 58 <i>b</i>	0.0180 86 47 <i>a</i> *	0.0089 86 -43 <i>c</i>		
M3 V _{Ga2}	2O ₁	0.0349 88 69 <i>c</i>	0.0180 80 -20 <i>a</i> *	0.0160 10 -30 <i>b</i>	2 2	-16 -21
M4 V _{Ga1} - Ga _{ib} - V _{Ga1} 160	O ₁	0.0228 0 <i>b</i>	0.0124 90 <i>c</i>	0.0025 90 <i>a</i> *	2	-21
M4' V _{Ga1} - Ga _{ib} - V _{Ga1} 160	2O ₁	0.0316 0 <i>b</i>	0.0140 90 <i>c</i>	0.0008 90 <i>a</i> *	4	-16 ^a
M5 V _{Ga1} - Ga _{ic} - V _{Ga1} 160	O ₃	0.0187 0 <i>b</i>	0.0177 90 <i>a</i> *	0.0036 90 <i>c</i>	2 1	-21 -20
M6 V _{Ga1} - Ga _{ia} - V _{Ga2} 160	O ₂	0.0342 69 -2 <i>a</i> *	0.0125 21 -4 <i>b</i>	0.0029 89 88 <i>c</i>	1 1	-27 -20

^a In PBE the *A* was -20.7 and in PBE+U it was impossible to keep the spins spread over the two sides, but in M4, PBE to PBE+U gave a reduction of *A* by a factor 20.7/26.7 = 0.775. Hence we reduced the PBE (M4') value by this factor.

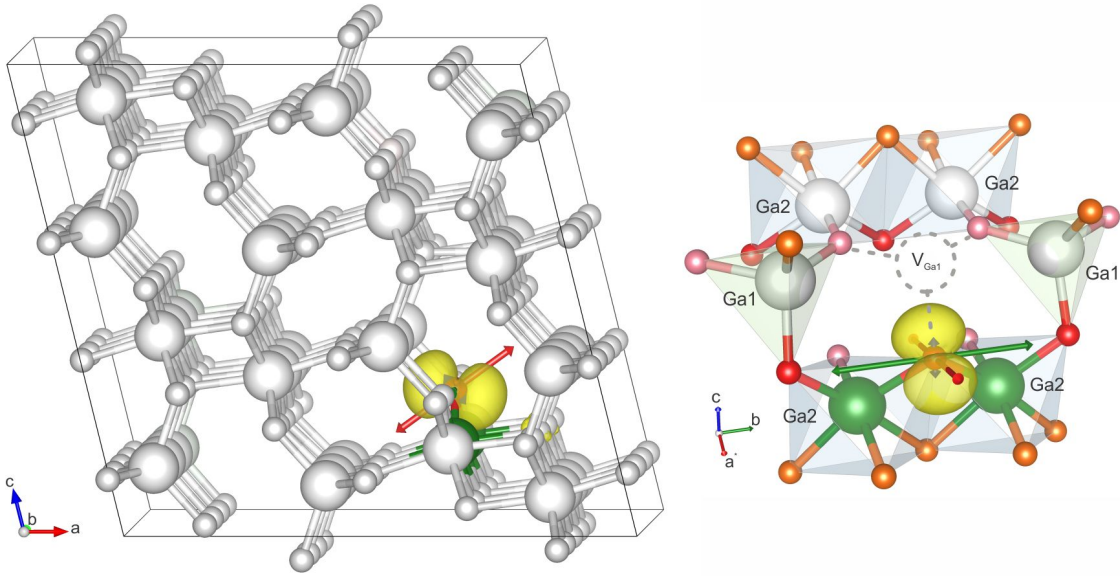


FIG. 7. V_{Ga1} (M1) structure, spin density in yellow, g -tensor principal axes indicated by double arrows with length proportional to the Δg (deviation from free electron value $g_e = 2.002391$), green colored Ga atoms are the ones with strong HFI. On the left it is viewed in the supercell, on the right the local structure is viewed from a different angle, the small O spheres are color coded red O₁, pink O₂, orange O₃ and the polyhedra surrounding the Ga and their type are indicated.

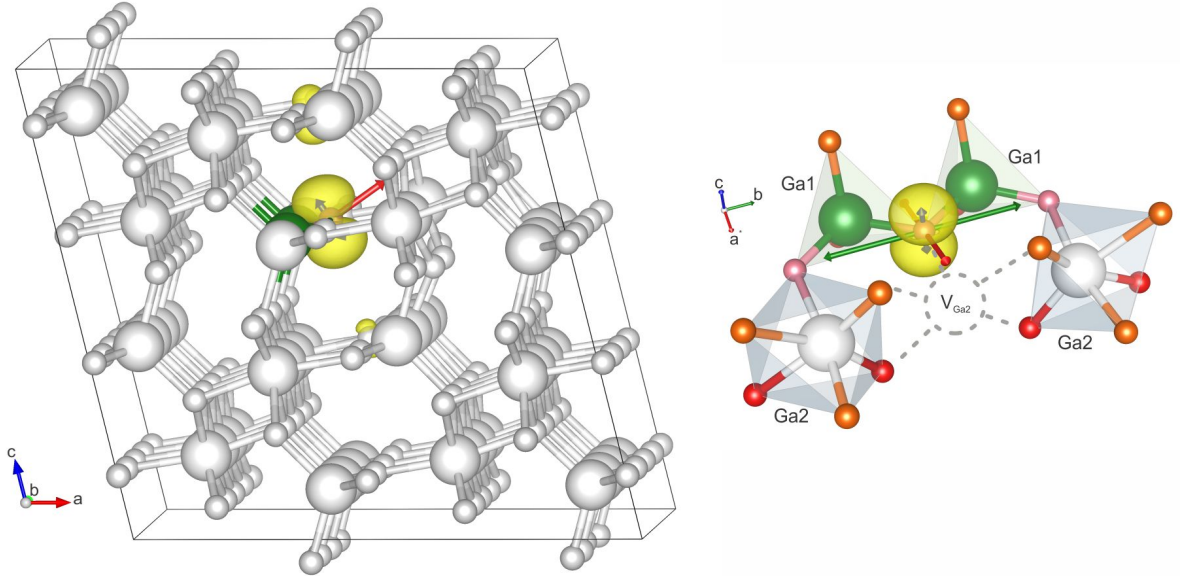


FIG. 8. V_{Ga2} (M2) structure, spin density in yellow, g -tensor and Ga atoms with strong HFI. See Fig. 7 for details.

VII. DISCUSSION

A. Models for EPR1

We now compare the calculated results with the experimental results. Starting with the simple V_{Ga} models, we first note that both V_{Ga1} and V_{Ga2} in their symmetric states have the main g -tensor component along the **b** direction in agreement with the experimental data for EPR1. Comparison between the results for two different

supercell sizes gives us an indication of the error bar introduced by the supercell size which apparently is about 0.001-0.002 in the g -tensor principal values. It also indicates some variation in the directions of the g -tensor. This is true for both V_{Ga1} and V_{Ga2} . The g -tensor however differs from the experimental one in two respects: first, the calculated one has a large, an intermediate and a small eigenvalue, whereas the experimental one has only one large Δg and two close significantly smaller values. Second, the smallest g principal value direction in the

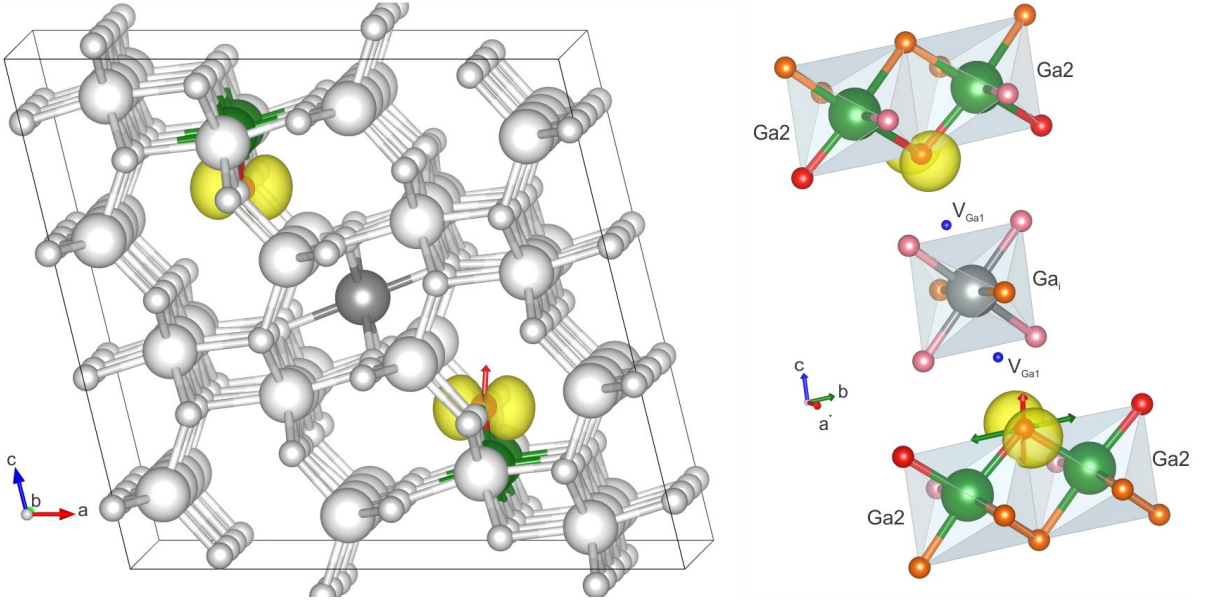


FIG. 9. $V_{\text{Ga1}} - \text{Ga}_{ib} - V_{\text{Ga1}}$ ($M4'$) structure, spin density in yellow, g -tensor principal axes (green is larger component, red intermediate) and Ga atoms with strong HFI. Details as in Fig. 7.

TABLE IV. EPR parameters for self-trapped holes, oxygen interstitial and related models. The table is arranged similar to Table III.

Model	O	g -tensor			HFI	
description cell	type	Δg_1	Δg_2	Δg_3	#Ga	A (G)
		θ_1	θ_2	θ_3		
		ϕ_1	ϕ_2	ϕ_3		
M7	O_1	0.0214	0.0205	0.0090	2	−8
STH $h_{O_1}^+$		90	0	90	1	−16
160		−73		17		
		c	b	a_*		
M8	$2O_2$	0.0172	0.0112	0.0042	2	−13
STH $h_{2O_2}^+$		0	90	90	2	−12
160			−2	88	2	−9
		b	a_*	c		
M9	O_1+O_i	0.0283	0.0037	0.0011	2	−8
O_i		90	0	90	1	−19
160		−79		11		
		c	b	a_*		
M10	O_i	0.0241	0.0051	0.0008	2	−3
$O_i - V_{\text{Ga1}}$		90	0	90		
160		84		−7		
		c	b	a_*		

calculation is close to \mathbf{c} (within about 20°), while in the experiment it is along \mathbf{a}_* . The direction of the smallest g -component can be seen to correspond to the direction of the p -like spin density (see *e.g.* Fig. 8).

In spite of these shortcomings and considering the uncertainties in Δg and its principal directions for the smaller Δg components, it is remarkable that both types of Ga vacancies give very similar results and in reasonable agreement with the major features of the experiment.

The largest g component means the largest spin-splitting for this direction of magnetic field and hence the smallest magnitude of the field at which the resonance occurs.

The hyperfine splitting for both of these models is on the two Ga atoms that are connected to the spin-carrying O. The values given are for the ^{69}Ga isotope. Their relative direction (which is along \mathbf{b}) in fact coincides with the maximum of the g -tensor. The fact that the hyperfine is on two Ga neighbors agrees with experiment but its value is overestimated in the calculation relative to the experiment by about 60 %. We should note that this result corresponds to a value of $U = 4$ eV. Within pure PBE-GGA, its value is even higher (about -29 G), while with a larger $U = 8$ eV it was reduced to -17 G, closer to the experimental value. Note that the sign is not determined by the experiment.

Next, we consider the various Ga-vacancy-pair Ga-interstitial complexes models M4-M6 (Fig. 9 and supplementary information⁴⁰). Among these, it is clear that only M4 and M4' give reasonable agreement with experiment. M5 has hyperfine interaction with three Ga and its g -tensor has two almost equal large values 0.018 along \mathbf{b} and \mathbf{a}_* in disagreement with both EPR1 and EPR2. M6 has its largest value along \mathbf{a}_* , the spin spread over two equivalent O_2 and significantly different hyperfine on two pairs of Ga. In contrast, M4 (Fig. 9) has a g -tensor maximum value along \mathbf{b} , the next along \mathbf{c} and the smallest along \mathbf{a}_* , in agreement with the experiment. In M4', where the spin is spread equally over the two O_1 far away from each other because on either side of the complex, the maximum g value along \mathbf{b} is further increased to $g_b \approx 0.03$ closer to the experiment and the intermediate value is reduced compared to the individual V_{Ga1} . Finally, its hyperfine is also reduced by the

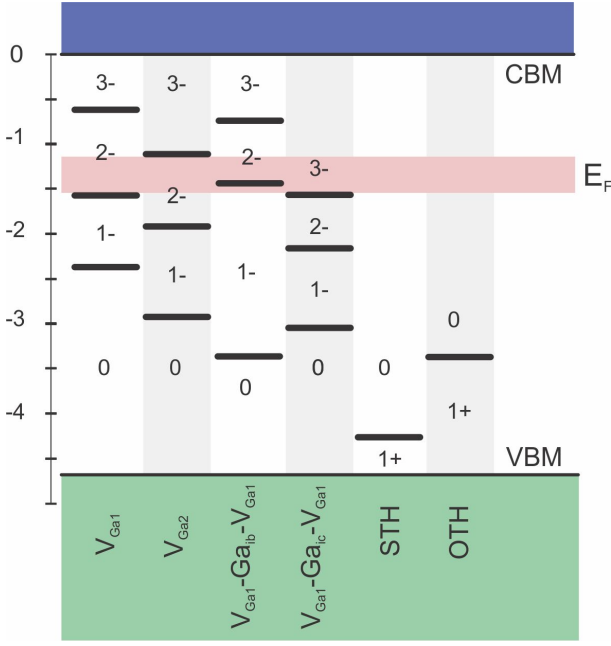


FIG. 10. Transition levels in the gap and expected Fermi level range after irradiation.

TABLE V. Transition levels of various defects relative to the conduction band minimum (in eV).

	V_{Ga1}	V_{Ga2}	(b)-complex	(c)-complex
2-/3-	-0.67	-1.16	-0.74	-1.59
1-/2-	-1.63	-1.91	-1.42	-2.20
0/1-	-2.35	-2.90	-3.34	-3.06

dynamic spreading over the two sites. Thus, this model appears to be the best candidate for the EPR1 spectrum.

However, we need to discuss now why only this variant of the V_{Ga1} would be seen in experiment or whether the experiment could be an average over several of these models. First, we note here that in order to be EPR observable the defect needs to be in the $q = -2$ charge state. In n-type conducting $\beta\text{-Ga}_2\text{O}_3$ the V_{Ga} are expected to be all in the $q = -3$ charge state, with all the O-dangling bond like states near the VBM completely filled. After irradiation, the Fermi level is expected to be lower in the gap, but we do not know exactly how deep. Furthermore, there might be local fluctuations in the Fermi level due to disorder. The calculated positions of the transition levels for different relevant models are shown in Fig. 10 and a tentative range of allowed Fermi levels is indicated keeping the above cautions in mind. The transition levels are also given numerically in Table V. We can see that both the V_{Ga1} and (b)-complex $V_{\text{Ga1}} - \text{Ga}_{ib} - V_{\text{Ga1}}$ have 2-/3- levels less deep below the conduction band minimum (CBM) at -0.67 eV and -0.74 eV respectively. It is thus plausible that the V_{Ga2} and the (c)-complex (even though it has lower total energy) are still in the $q = -3$

EPR inactive state. The position of these levels is somewhat deeper in other calculations^{10,11,19} but all calculations agree that the V_{Ga2} is deeper than the V_{Ga1} . Now, between the V_{Ga1} and the related M4 or (b)-complex, the latter has lower energy in the $q = -2$ state (see Table II) and can spontaneously occur with only a small migration barrier to overcome. One may indeed consider it as the ground states of this V_{Ga1}^{-2} state. This leads us to assign EPR1 to the M4 or M4'. Whether the hyperfine is spread over two equivalent Ga or over two pairs of these leads to only minor differences in the nature of the simulated hyperfine spectrum. The experiment appears to be better fit with two rather than four equivalent Ga, indicating that the spin is localized on one side. The calculations also favor this model. On the other hand, spreading the spin over the two gives somewhat reduced hyperfine tensor values. We may consider the spread over the two sites as a dynamical effect which lowers the value of the hyperfine interaction. As mentioned earlier we need rather high values of U in PBE+ U to obtain agreement with the experimental hyperfine values.

B. Models for EPR2

Next, we consider the possible candidates for EPR2. Now that we have established that the largest g -tensor direction in these defects tends to correspond to the pair of Ga connected to the spin carrying O atom, it becomes clear that few candidates can lead to a g -tensor with maximum along **c**. Only the tilted spin model M3 is a candidate among the Ga-vacancy type defects. Its spin density and g -tensor and HFI are shown in Fig. 11. The reason is that in this case the directions of the Ga pairs which are in between **b** and **c** become averaged over the two mirror-related pairs on either side of the mirror plane. In fact, in the calculations we observed that the self-consistent solution of the spin density could easily flop from one side to the other and be located on only one. Therefore we can consider two models: either the spin is indeed on only one of the two O but two variants of it occur in the sample and need to be averaged over. Or, the spin is really flopping from one to the other in a given defect by dynamic coupling to a local vibrational mode. In some sense, this is what we simulate in M3 by enforcing it to have the spin symmetrically located on the two O. While this model than has interaction with 4 spins, there are two slightly nonequivalent pairs. Their hyperfine splitting differs by only 5 G and this may still be a bit of an overestimate. Thus, this may still fit the experimental observation where for simplicity a fit was made with two equivalent Ga A parameters and gave a better agreement with experiment than allowing for two different sets of Ga hyperfine parameters. In terms of the g -tensor, this model has the largest value along **c** in agreement with experiment, but the next smaller value is along **a**_{*} rather than **b**. Again, this type of small deviations from experiment may be considered to fall within

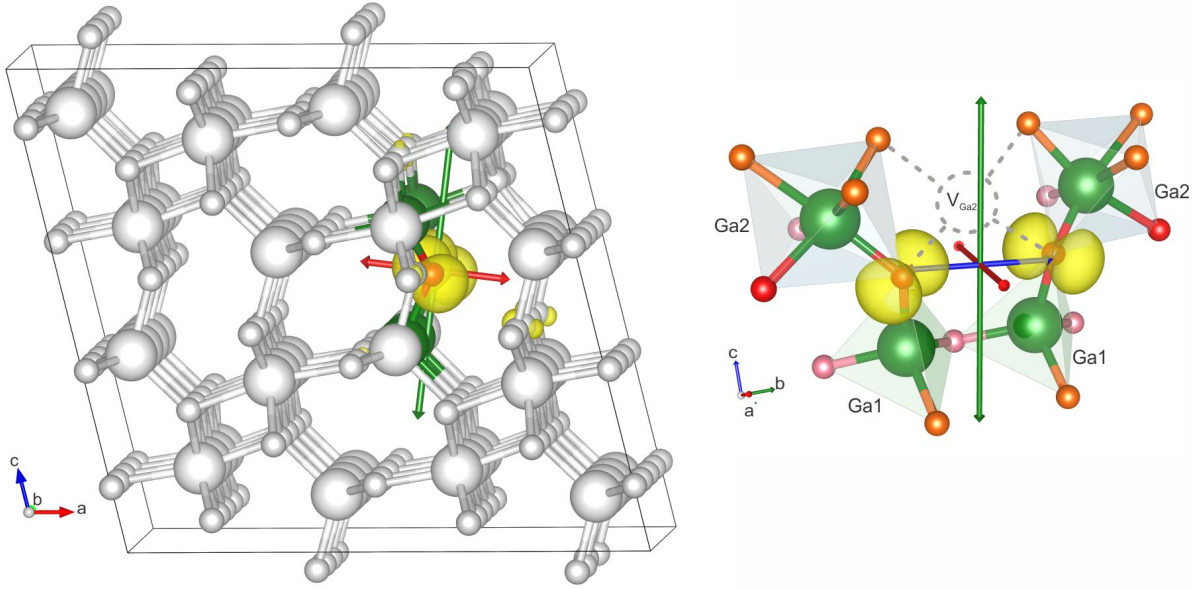


FIG. 11. Model M3 with tilted spins for $V_{\text{Ga}2}$ structure, spin density, g -tensor and Ga atoms with strong HFI. Details as in Fig. 7.

the error bar of the calculations. Thus M3 appears to be a reasonable model for EPR2.

Next, because the M3 model is still not perfectly fitting, we consider some of the alternative models based on self-trapped holes of interstitial O. First consider the M7 self-trapped hole model with the hole trapped on O_1 and which was previously proposed to be the origin of this spectrum.¹⁸ Its g -tensor has indeed principal value directions close to \mathbf{c} , followed by \mathbf{b} and \mathbf{a}_* . However the values of $g_c \approx g_b \gg g_{a*}$. More importantly, there is strong hyperfine interaction with three Ga and the strongest component is actually along the third single Ga. The next model M8 with holes trapped on two adjacent O_2 has hyperfine with 6 Ga and nonmatching g -tensor and can easily be dismissed. A figure for this model can be found in supplementary information.⁴⁰

The O_i M9 model on the other hand (shown in Fig. 13) has a g -tensor that matches the experiment quite well in terms of the order of the principal axes, $g_c \gg g_b \approx g_{a*}$ although Δg_c is still a bit small. The HFI with the pair of equivalent Ga_2 next to the O_1 position is also in good agreement (8 G calculated vs. 9.4 G), although it is a bit surprising to find a lower rather than higher value compared with experiment, for $U = 4$ eV compared to the other cases. However, as can be seen in Fig. 13, we find the spin density to be in a π like orbital spread over the two O atoms in the dumbbell and hence there is also a strong HFI with the third Ga, which is in fact, higher. This does not fit the experiment. We find that the hyperfine tensor on the third Ga is strongly anisotropic and is rather sensitive to the position of the third Ga. However, the measured hyperfine splitting for the EPR2 spectrum is almost isotropic and no signs of a third Ga with discernible hyperfine interaction is found.

Simulations with a pair of equivalent Ga plus a third Ga hyperfine show that the effects of the third Ga should be clearly visible even for a small hyperfine A . So, this model has some attractive features in terms of the g -tensor but can be ruled out on the basis of the absence of a third Ga hyperfine interaction in the experiment.

As a further modification of this model, we removed the third Ga from M9 and thereby created model M10, shown in supplementary information.⁴⁰ In that case, the spin becomes more pulled toward the O farther away from the Ga_2 pair, and the HFI on them becomes too small but the g -tensor stays similar. The too small hyperfine splitting invalidates this model as a candidate.

Finally, referring back to Fig. 10 we note that the self-trapped hole as well as the split-interstitial O_i models have much deeper transition levels to the EPR active positive charge states. While this does not completely exclude them, it makes them much less likely candidates.

C. $S = 1$ spectra

Several of the defects were calculated in the $q = -1$ state in order to assign the $S = 1$ spectra. It was found that for the simple $V_{\text{Ga}1}$ model, the second hole tends to localize on the pair of O_2 rather than the O_3 on the mirror plane. This would break the symmetry and not be consistent with an $S = 1$ very closely related to the $S = 1/2$ EPR1 spectrum. Similar considerations hold for $V_{\text{Ga}2}$ when starting from the symmetric solution with spin on O_2 on the mirror plane (M2). On the other hand, the (b)-complex $V_{\text{Ga}1} - \text{Ga}_{ib} - V_{\text{Ga}1}$ or M4 model is an ideal candidate for the $S = 1$ spectrum. First, the spins on the O_1 type atoms near each $V_{\text{Ga}1}$ in this model are far apart

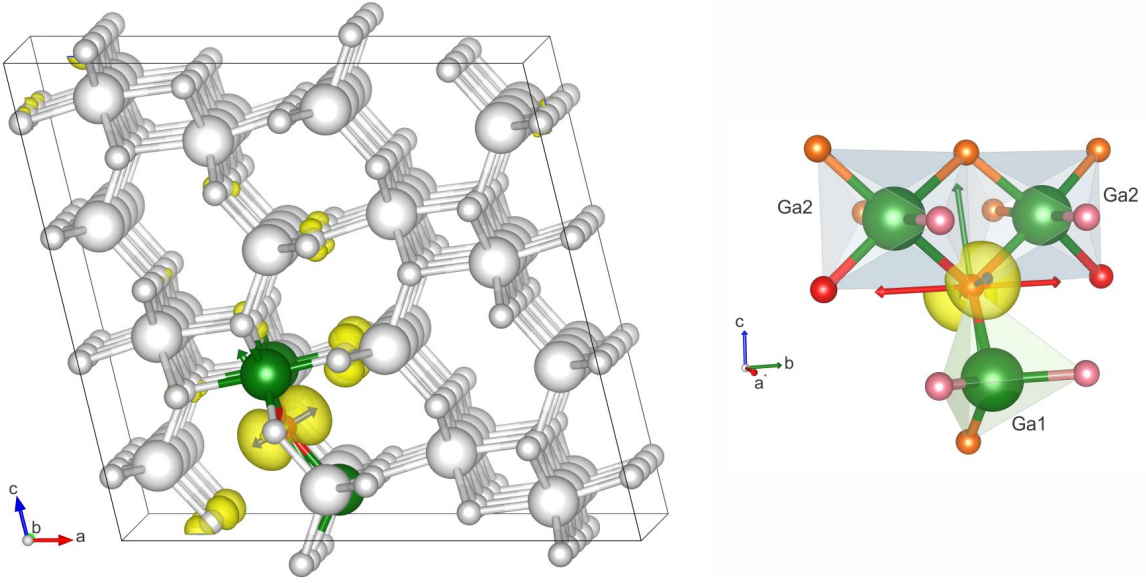


FIG. 12. Self-trapped polaron spin density on O_1 (Model M7) in yellow, g -tensor (double arrows) and Ga exhibiting strong HFI. Details as in Fig. 7

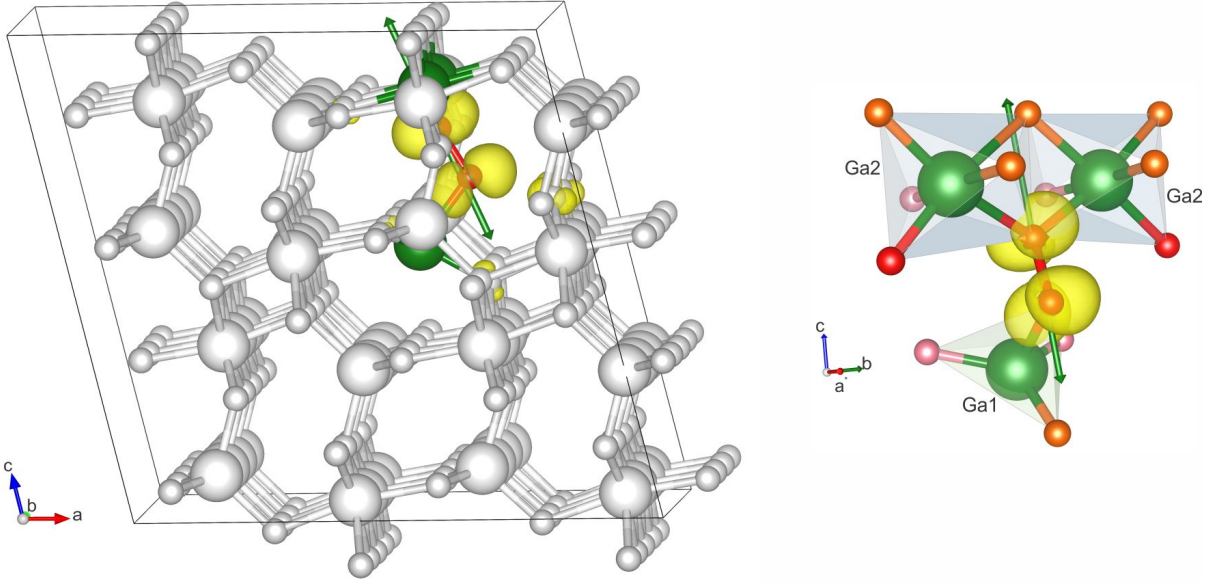


FIG. 13. Interstitial O_i with O-O dumbbell oriented along c (M9) structure, spin density in yellow, g -tensor (double arrows) and Ga exhibiting strong HFI. Details as in Fig. 7

(~ 7.3 Å), so that this would indeed correspond to two weakly interacting spins. Second, this $S = 1$ $q = -1$ state was indeed found to have halved hyperfine interactions compared to the $S = 1/2$ and a similar g -tensor with maximum along b of $\Delta g_b = 0.0316$, $\Delta g_2 = 0.014$ close to (about 17° from) the c -axis and $\Delta g_3 = 0.007$ close to a_* . Third, this particular complex, has lowest energy among all the Ga-vacancy related models in the $q = -1$ charge state. Thus the occurrence of this $S = 1$ spectrum further confirms the identification of EPR1 with the (b)-

complex form of the V_{Ga1} .

As for the EPR2 related $S = 1$ state, the M3 model is still a plausible model to catch a second hole. We found the $S = 1$ state of M3 with $q = -1$ to have a similar g -tensor $\Delta g_1 = 0.037$, $\theta_1 = 90^\circ$, $\phi_1 = 56^\circ$, close to c -axis, $\Delta g_2 = 0.0245$, $\theta = 0$ (b -axis), and $\Delta g_3 = 0.0154$, $\theta_3 = 90^\circ$, $\phi_3 = -34^\circ$ (closer to a_*) as the the $S = 1/2$ symmetric model. However, there is somewhat larger interaction between the spins in this model because the O are only 3.5 Å apart. This leads to somewhat more dif-

ference between the nonequivalent Ga atoms which now have hyperfine contact terms of 12 G and 27 G instead of 16 G and 21 G in the $S = 1/2$. This is less clearly indicative of weakly coupled spins. We note also that this newly found EPR2 $S = 1$ spectrum has a more complex lineshape with a broad line underlying the halved hyperfine splitting of the $S = 1/2$ part of the spectrum. This broadening could possibly be explained by the two sets of equivalent pairs involved in this spectrum.

The O_i is very unlikely to have an associated $S = 1$ $q = +2$ charge state. The $q = +2$ state can safely be dismissed on the ground of total energy calculations.

D. Photoexcitation process

The nature of the photoexcitation process and the meaning of the threshold value are discussed next. If we consider the EPR2 to be related to V_{Ga2} in the M3 model, we may consider a migration path of Ga for converting the M4 model to M3. Following Kyrtos *et al.*¹⁹ the migration barrier for from Ga in the i_b site to a Ga_1 site via a $q9$ jump is 1.0 eV in the $q = -2$ charge state. We are then left with a single V_{Ga1} , which could migrate to one the neighboring octahedral sites by a $q6$, $q8$, $q10$ or $q4 + q5$ paths (following the notation of Ref. 19). These would add an additional 1.2-1.7 eV. So, the total energy to transform the M4 to a V_{Ga2} path would amount to about 2.5 ± 0.3 eV. This agrees rather well with the photo threshold. It is still not clear why following these transition paths we would end up in the metastable state of the V_{Ga2} with spin distributed off the mirror plane but given these dynamic processes, this does not seem too implausible. In the above model, the photoexcitation process is viewed as a direct transformation of the defect from one form to the other related to V_{Ga} migration.

On the other hand, the photoexcitation process may also be considered to in some way lower the effective Fermi level and indirectly transfer the hole from one defect center to another. The nature of the barrier or threshold for this process is less clear.

We might for example consider a direct transfer of an electron from a O_i site to the V_{Ga1} or the related (b)-complex by means of the photoexcitation process. Since the former has a $+/0$ level at about 1.6 eV above the VBM and the latter a $2 - /3 -$ at about 4.0 eV above the VBM, an energy of about 2.4 eV is required for this transfer, again a value close to the threshold. Thereby the V_{Ga1} is then EPR inactivated and the O_i activated, because we can view it as the hole moving the opposite way. It is however, not so clear how this transfer of the carriers between possibly more remote sites is happening in response to the photoexcitation. This latter model for the photoexcitation process would seem to be in support of the split-interstitial O_i . However, we have already given arguments earlier why this is a less likely model for the EPR2 spectrum. Among other it does not have a corresponding $S = 1$ spectrum and is expected to have a

more complex hyperfine splitting with some effects of a third Ga.

Overall, the Ga-vacancy migration type model seems a more likely process for the photoexcitation of the EPR2 model. We should however keep in mind that apparently¹⁸ this EPR center can also be created by X-ray absorption at low temperature starting from the EPR1 containing sample. So, the meaning of the photothreshold is not entirely clear. The computational result that the M3 model is actually not the lowest energy state of the V_{Ga2} but a metastable state, could in part explain why this EPR2 center disappears above a certain temperature. The corresponding V_{Ga2} in the M2 symmetric model, if it becomes allowed thereby at lower Fermi level position, would still have a g -tensor with maximum along b and therefore closely resemble that of EPR1. Eventually, we may expect that further migration process would return the system to the lowest energy (b)-model complex assigned to EPR1.

VIII. CONCLUSIONS

A combined experimental/theoretical EPR study was carried out on β - Ga_2O_3 single crystals in order to unravel the potentially V_{Ga} -related EPR spectra observed in this material. After high energy electron or proton irradiation, the samples show an $S = 1/2$ spectrum (labeled EPR1) at room temperature or below, characteristic of a oxygen localized spin density with hyperfine on two equivalent Ga atoms and the largest g -tensor component's principal axis along the \mathbf{b} axis of the crystal. This spectrum is the same as previously reported after neutron irradiation.¹⁶ Photoexcitation with a threshold of 2.8 eV is shown to change the EPR center to a different orientation of the g -tensor with main axis along \mathbf{c} (labeled EPR2) and slightly smaller hyperfine splitting. This center remains stable up to 120 K after which the original one is reversibly restored. This center is the same as previously reported in Ref. 18 to occur after X-ray excitation at low temperature. Each of these $S = 1/2$ centers is also accompanied by an $S = 1$ spectrum with the same g -tensor and about half the hyperfine splitting, thus indicating two weakly interacting $S = 1/2$. Their zero-field splitting indicates a single well-defined distance between the two weakly interacting $S = 1/2$ spins. The $S = 1$ portion of the spectrum is weaker before than after the photoexcitation.

First-principles calculations of the g -tensor and hyperfine tensors were carried out for a wide variety of models of intrinsic defects. Both the tetrahedral V_{Ga1} and octahedral V_{Ga2} Ga-vacancies have a ground state with spin localized on a single oxygen located on the mirror-plane m_b perpendicular to \mathbf{b} and have the principal component of the g -tensor along the \mathbf{b} direction. However, their smallest component is found along \mathbf{c} while the experimental one is along \mathbf{a}_* and the calculated Δg -tensor shows three about equally spaced eigenvalues while the

experiment has one large and two small g -eigenvalues. A closely related complex, the $V_{\text{Ga1}} - \text{Ga}_{ib} - V_{\text{Ga1}}$ with orientation along a direction intermediate between \mathbf{a}_* and \mathbf{c} has a g -tensor qualitatively closer to EPR1 in terms of its principal axis orientations and has lower energy than the simple V_{Ga1} . Another complex (labeled (c)), which is differently oriented, has hyperfine spread over three Ga and is thereby excluded as model for EPR1. Furthermore, we find that the $q = -2$ charge state which is the $S = 1/2$ EPR active state is accessible to the (b) complex at a Fermi level position less deep below the CBM than for the other complex. We thus assign EPR1 to the (b) complex under the assumption that the competing (c)-complex would still be in a non-EPR active state.

The V_{Ga2} has a metastable state with spin localized on a pair of oxygens off the mirror plane or a single oxygen on either side of the mirror plane. This model or the average of the two would give the main g -tensor direction along \mathbf{c} and is thus a good candidate for EPR2. However, it has hyperfine interaction with two pairs of slightly nonequivalent Ga and the smaller components of the calculated g -tensor do not match the experiment precisely.

Both the above models can readily also occur in a single negatively charged ($q = -1$) state with $S = 1$ and in particular for the EPR1 spectrum, this leads to a model of weakly interacting spins consistent with the experiment. For EPR2, the interaction of the spins would be somewhat stronger and perturb the system more. The photoexcitation process is proposed to be related to the Ga migration processes that convert the EPR1 center into the EPR2 center.

A self-trapped hole has been suggested as another model for the EPR2 center previously observed. It is ruled out on the basis of its non-matching g -tensor and hyperfine with three Ga atoms. Oxygen interstitials form a split interstitial O_2 dumbbell located on an O site. In the neutral state, this dumbbell is oriented along the \mathbf{c} direction while in the $q = +1$ charge state, its ground state

has the dumbbell rotated to the \mathbf{b} direction. However, if the \mathbf{c} oriented dumbbell captures a hole, and remains in this metastable orientation, it is found to have a g -tensor which best of all matches the EPR2 center. Namely it has one large component along \mathbf{c} and two smaller ones along \mathbf{c} and \mathbf{a}_* . It has strong hyperfine with two equivalent Ga plus a third one that depends strongly on the location of that Ga which moves in a flat potential and has a very anisotropic hyperfine tensor on the third Ga. Although this model has a g -tensor fitting the experiment, the predicted hyperfine interaction with three Ga is not found in the experiment and rules out this model. This EPR center is also less likely to occur because the required $q = +1$ charge state of that defect occurs deeper below the CBM and a corresponding $S = 1$ center, which would require a $q = +2$ state is not possible.

Further work is required to fully analyze the $S = 1$ spectra and zero-field splitting. It would also be very interesting to look for methods to push the Fermi level deeper below the CBM and thereby activating the O_i related and potentially also other so far hidden V_{Ga} related EPR spectra.

ACKNOWLEDGMENTS

The work at CWRU was supported by the National Science Foundation under grant No. DMR-1708593. The calculations were carried out at the Ohio Supercomputer Center under Project No. PAA0032. The work at BC-CMS was supported by the DFG grant No. FR2833/63-1 and by the Supercomputer Center of Northern Germany (HLRN Grant No. hbc00027). U.G. acknowledges support by the Deutsche Forschungsgemeinschaft (DFG) priority program SPP-1601. We acknowledge the Helmholtz Zentrum Dresden (HZDR) in Rossendorf (Germany) for the proton and electron irradiation and the laboratory CEMHTI, CNRS, Orlans (France) for proton irradiation.

- ¹ K. Sasaki, M. Higashiwaki, A. Kuramata, T. Masui, and S. Yamakoshi, *J. Cryst. Growth* **378**, 591 (2013), the 17th International Conference on Molecular Beam Epitaxy.
- ² T. Matsumoto, M. Aoki, A. Kinoshita, and T. Aono, *Jap. J. Appl. Phys.* **13**, 1578 (1974).
- ³ H. Peelaers and C. G. Van de Walle, *Phys. Status Solidi (b)* **252**, 828 (2015).
- ⁴ J. Furthmüller and F. Bechstedt, *Phys. Rev. B* **93**, 115204 (2016).
- ⁵ K. A. Mengle, G. Shi, D. Bayerl, and E. Kioupakis, *Appl. Phys. Lett.* **109**, 212104 (2016), <http://dx.doi.org/10.1063/1.4968822>.
- ⁶ A. Ratnaparkhe and W. R. L. Lambrecht, *Applied Physics Letters* **110**, 132103 (2017), <http://dx.doi.org/10.1063/1.4978668>.
- ⁷ A. J. Green, K. D. Chabak, E. R. Heller, R. C.

- Fitch, M. Baldini, A. Fiedler, K. Irmscher, G. Wagner, Z. Galazka, S. E. Tetlak, A. Crespo, K. Leedy, and G. H. Jessen, *IEEE Electron Device Letters* **37**, 902 (2016).
- ⁸ B. J. Baliga, *IEEE Electron Device Letters* **10**, 455 (1989).
- ⁹ H. Peelaers, D. Steiauf, J. B. Varley, A. Janotti, and C. G. Van de Walle, *Phys. Rev. B* **92**, 085206 (2015).
- ¹⁰ J. B. Varley, H. Peelaers, A. Janotti, and C. G. Van de Walle, *J. Phys. Condens. Matter* **23**, 334212 (2011).
- ¹¹ J. B. Varley, A. Janotti, C. Franchini, and C. G. Van de Walle, *Phys. Rev. B* **85**, 081109 (2012).
- ¹² T. Harwig and F. Kellendonk, *J. Solid State Chem.* **24**, 255 (1978).
- ¹³ T. Zacherle, P. C. Schmidt, and M. Martin, *Phys. Rev. B* **87**, 235206 (2013).
- ¹⁴ H. Peelaers and C. G. Van de Walle, *Phys. Rev. B* **94**, 195203 (2016).

- ¹⁵ P. Deák, Q. Duy Ho, F. Seemann, B. Aradi, M. Lorke, and T. Frauenheim, *Phys. Rev. B* **95**, 075208 (2017).
- ¹⁶ B. E. Kananen, L. E. Halliburton, K. T. Stevens, G. K. Foundos, and N. C. Giles, *Applied Physics Letters* **110**, 202104 (2017), <http://dx.doi.org/10.1063/1.4983814>.
- ¹⁷ S. Geller, *J. Chem. Phys.* **33**, 676 (1960), <http://dx.doi.org/10.1063/1.1731237>.
- ¹⁸ B. E. Kananen, N. C. Giles, L. E. Halliburton, G. K. Foundos, K. B. Chang, and K. T. Stevens, *Journal of Applied Physics* **122**, 215703 (2017), <https://doi.org/10.1063/1.5007095>.
- ¹⁹ A. Kyrtos, M. Matsubara, and E. Bellotti, *Phys. Rev. B* **95**, 245202 (2017).
- ²⁰ C. J. Pickard and F. Mauri, *Phys. Rev. B* **63**, 245101 (2001).
- ²¹ C. J. Pickard and F. Mauri, *Phys. Rev. Lett.* **88**, 086403 (2002).
- ²² H. J. von Bardeleben, J. L. Cantin, U. Gerstmann, A. Scholle, S. Greulich-Weber, E. Rauls, M. Landmann, W. G. Schmidt, A. Gentils, J. Botsoa, and M. F. Barthe, *Phys. Rev. Lett.* **109**, 206402 (2012).
- ²³ H. J. von Bardeleben, J. L. Cantin, H. Vrielinck, F. Callens, L. Binet, E. Rauls, and U. Gerstmann, *Phys. Rev. B* **90**, 085203 (2014).
- ²⁴ G. Pfanner, C. Freysoldt, J. Neugebauer, and U. Gerstmann, *Phys. Rev. B* **85**, 195202 (2012).
- ²⁵ U. Gerstmann, M. Rohrmüller, F. Mauri, and W. Schmidt, *Physica Status Solidi (c)* **7**, 157 (2010).
- ²⁶ D. Ceresoli, U. Gerstmann, A. P. Seitsonen, and F. Mauri, *Phys. Rev. B* **81**, 060409 (2010).
- ²⁷ <http://qe-forge.org/gf/project/qe-gipaw/>.
- ²⁸ P. Giannozzi, S. Baroni, N. Bonini, M. Calandra, R. Car, C. Cavazzoni, D. Ceresoli, G. L. Chiarotti, M. Cococcioni, I. Dabo, A. Dal Corso, S. de Gironcoli, S. Fabris, G. Fratesi, R. Gebauer, U. Gerstmann, C. Gougousis, A. Kokalj, M. Lazzeri, L. Martin-Samos, N. Marzari, F. Mauri, R. Mazzarello, S. Paolini, A. Pasquarello, L. Paulatto, C. Sbraccia, S. Scandolo, G. Sclauszero, A. P. Seitsonen, A. Smogunov, P. Umari, and R. M. Wentzcovitch, *Journal of Physics: Condensed Matter* **21**, 395502 (19pp) (2009).
- ²⁹ J. P. Perdew, K. Burke, and M. Ernzerhof, *Phys. Rev. Lett.* **77**, 3865 (1996).
- ³⁰ J. Heyd, G. E. Scuseria, and M. Ernzerhof, *J. Chem. Phys.* **118**, 8207 (2003).
- ³¹ J. Heyd, G. E. Scuseria, and M. Ernzerhof, *J. Chem. Phys.* **124**, 219906 (2006).
- ³² J. P. Perdew, M. Ernzerhof, and K. Burke, *J. Chem. Phys.* **105**, 9982 (1996).
- ³³ <http://www.quantum-espresso.org/>.
- ³⁴ G. Kresse and J. Furthmüller, *Computational Materials Science* **6**, 15 (1996).
- ³⁵ G. Kresse and D. Joubert, *Phys. Rev. B* **59**, 1758 (1999).
- ³⁶ <https://www.vasp.at/>.
- ³⁷ S. Blügel, H. Akai, R. Zeller, and P. H. Dederichs, *Phys. Rev. B* **35**, 3271 (1987).
- ³⁸ C. G. Van de Walle and P. E. Blöchl, *Phys. Rev. B* **47**, 4244 (1993).
- ³⁹ M. S. Bahrany, M. H. F. Sluiter, and Y. Kawazoe, *Phys. Rev. B* **76**, 035124 (2007).
- ⁴⁰ The Supplementary Information contains additional figures of the spin density, g -tensor and large hyperfine atoms for some of the models, not shown in the main text. Also VESTA files which allow to view these structures from different angles are provided.